Chaos, Solitons & Fractals 52 (2013) 59–65

Contents lists available at SciVerse ScienceDirect

Chaos, Solitons & Fractals

Nonlinear Science, and Nonequilibrium and Complex Phenomena

journal homepage: www.elsevier.com/locate/chaos

Periodicity hubs and wide spirals in a two-component autonomous electronic circuit

Cecilia Cabeza [a], Carlos A. Briozzo [a], Rodrigo Garcia [a], Joana G. Freire [b,c,d], Arturo C. Marti [a,b], Jason A.C. Gallas [a,b,c,d,e,*]

[a] Instituto de Física, Facultad de Ciencias, Universidad de la República, Iguá 4225, Montevideo, Uruguay
[b] Departamento de Física, Universidade Federal da Paraíba, 58051-970 João Pessoa, Brazil
[c] Institute for Multiscale Simulations, Friedrich-Alexander-Universität Erlangen-Nürnberg, 91052 Erlangen, Germany
[d] Centro de Estruturas Lineares e Combinatórias, Faculdade de Ciências, Universidade de Lisboa, 1649-003 Lisboa, Portugal
[e] Instituto de Altos Estudos da Paraíba, Rua Infante Dom Henrique 100-1801, 58039-150 João Pessoa, Brazil

ARTICLE INFO

Article history:
Received 30 January 2013
Accepted 8 April 2013
Available online xxxx

ABSTRACT

We report an autonomous circuit containing periodicity hubs with surprisingly broad spirals. Knowledge of broad spirals is important because all presently known spirals are compressed along specific directions in parameter space making them difficult to study experimentally and theoretically. We characterize the performance of the circuit by computing stability diagrams for relevant sections of the control space. In addition, the alternation of chaotic and periodic spiral phases is contrasted with equivalent alternations obtained from an experimental implementation of the circuit.

1. Introduction

Numerical simulations have recently revealed a number of unexpected regularities in the control parameter space of dissipative flows [1–7]. These regularities consist of a wide-ranging alternation of an apparently infinite hierarchy of periodic and chaotic spiral phases which converge to certain focal points called *periodicity hubs*. Such hubs are accumulation points of a doubly infinite sequence of *spirals*: an infinite family of spirals characterized by parameters leading to periodic oscillations, intercalated with an infinite family of spirals of chaotic oscillations. Individual spirals of periodicity are composed by specific waveforms which evolve continuously along the spiral, with a period that approaches a specific value but with a number of spikes (local maxima) which seems to grow without any bound, diverging at the focal point.

Hubs and spirals were observed in systems as diverse as lasers, chemical oscillators, electronic circuits operating with either piecewise-linear or smooth nonlinearities, and in other systems covering a large spectrum of practical applications [2–4]. Periodicity hubs were found not to be isolated points but to emerge forming infinite *networks of points* organizing stable periodic and chaotic phases in flows [5–7]. An experimental demonstration involving an autonomous Duffing-like proxy displaying surprising *discontinuous spirals* was reported recently [8]. Networks of a rather distinct type, forming zig-zag patterns, were also described recently for a circuit with a tunnel diode, for a fiber-ring laser and for the Hénon map [9].

Of interest for applications is the fact that hubs are very robust against parameter changes and induce a wide-range of predictability in control parameter space. By constructing detailed phase diagrams, i.e. *stability charts*, displaying the precise location in parameter space of the dynamical phases, one obtains valuable information about how to perform accurate parameter changes and to effectively *control* the system. Note that this is different from just *perturbing* the system without a prescription to define which

* Corresponding author Address: Institute for Multiscale Simulations, Friedrich-Alexander-Universität Erlangen-Nürnberg, 91052 Erlangen, Germany.
E-mail address: jason.gallas@cbi.uni-erlangen.de (J.A.C. Gallas).

0960-0779/$ - see front matter © 2013 Elsevier Ltd. All rights reserved.
http://dx.doi.org/10.1016/j.chaos.2013.04.001

new dynamical state will emerge after parameter changes. Also of interest is that parameter charts allow one to perform big changes of control parameters, not just infinitesimally small changes as it is common nowadays.

From the experimental point of view, due to the fact that hubs and spirals usually emerge compressed and distorted, hubs and spirals are not always easy to detect. An additional reason is that to observe hubs and spirals one first needs to locate adequate parameter windows in an usually high-dimensional control parameter space. Parameter tuning is normally difficult to perform experimentally. In this case computer simulations help to expeditiously locate suitable regions to study hubs experimentally. An interesting additional byproduct of stability diagrams is that they may reveal shortcomings of the theoretical description of the electronic components (diodes, lasers, etc.) whenever discrepancies between computations and measurements emerge.

In this paper, we study numerically and experimentally a slight variation of a circuit investigated by Chua and Lin [10,11] and subsequently considered in this Journal by Kyprianidis et al. [12–14]. This circuit displays hubs with surprisingly wide spirals in sections of its control parameter space (see Figs. 3–5 below). The main novelty of our work is the discovery of wide spirals in the circuit. The discovery of wide spirals is important because known spirals emerge compressed along specific directions in parameter space making such distorted spirals particularly difficult to study experimentally and theoretically. We report high-resolution stability diagrams describing parameter sections containing hubs and wide spirals and specifying numerical values for hardware implementations. We also present stability diagrams obtained from a particular experimental implementation of the circuit.

In the next Section we introduce the circuit. In Section 3 we describe how the numerical simulations were done. Section 4 contains the bulk of stability diagrams while Section 5 describes how the experimental stability diagrams were obtained and compares them with numerical simulations. Finally, in Section 6 we summarize our results.

2. Electronic circuit

The electronic circuit studied here, shown schematically in Fig. 1, is governed by an autonomous system of four first-order ordinary differential equations. It involves two active elements, a nonlinear resistor *RN* (implemented using a Chua's diode [10,11]) and a negative conductance *GN*. Both elements exhibit symmetrical piecewise-linear $v-i$ characteristics as represented in Fig. 2. The main difference with the previous implementation by Kyprianidis et al. [12–14] is that our circuit takes into account the saturation effects of the real operational amplifier used in *GN*. We remark, however, that hubs and spirals can be also observed in the ideal model considered by Kyprianidis et al. [12–14]. The parameter values used in our experimental implementation and numerical simulations, unless stated otherwise, are the ones summarized in Table 1.

According to Kirchhoff's laws, the equations governing the circuit of Fig. 1 are given by

$$C_1\frac{dv_1}{dt} = i_1 - i_{RN}(v_1), \tag{1}$$

$$C_2\frac{dv_2}{dt} = -i_1 - i_2 - i_{GN}(v_2), \tag{2}$$

$$L_1\frac{di_1}{dt} = v_2 - v_1 - i_1R_1, \tag{3}$$

$$L_2\frac{di_2}{dt} = v_2 - i_2R_2, \tag{4}$$

where v_1 (resp. v_2) is the voltage across the capacitances C_1 (C_2) and i_1 (i_2) is the current through the inductance L_1 (L_2). The $v-i$ characteristics of the nonlinear elements are represented by the following expressions

$$i_{RN}(v_1) = G_c v_1 + \frac{1}{2}(G_a - G_b)(|v_1 + E_{1p}| - |v_1 - E_{1p}|) + \frac{1}{2}(G_b - G_c)(|v_1 + E_{2p}| - |v_1 - E_{2p}|), \tag{5}$$

$$i_{GN}(v_2) = G_{bb}v_2 + \frac{1}{2}(G_{aa} - G_{bb})(|v_2 + E_b| - |v_2 - E_b|). \tag{6}$$

The parameters in these equations are functions of the characteristics of the electronic components. In particular, E_b depends on the *output voltage swing*, V_{sat}, of the operational amplifier, and its input voltage, V_{cc} = 15 V. The different slopes of the nonlinear $v-i$ characteristics of *RN*, G_a and G_b, also depend on the non-zero forward voltage, V_γ, of the diodes which are modeled here as an ideal diode and a battery. Both parameters V_γ and V_{sat} and their uncertainties were estimated from the data sheet provided by the manufacturer. Although these parameters could present some variations with respect to the specified values, the manufacturer claims that they remain constant for each component. In part, these small differences could explain a global drift when comparing experiments and numerical simulations (see below).

Table 2 provides detailed explanation about how E_b, G_a, and G_b depend on V_{sat} and V_{cc} and an estimate of uncertainties involved in our measurements. Justifications for such dependencies are well-known [15]. In computing the values in Table 2 we used the representative values V_γ = 0.65 V and V_{sat} = 12.7 V, as estimated from the data sheet provided by the manufacturer, and V_{cc} = 15 V.

3. Numerical simulations

As mentioned in the introduction, before starting hardware experiments it is best to first perform numerical simulations in order to locate adequate parameter windows. This preliminary search is particularly important in systems like ours, which involve a high-dimensional control parameter space. As discussed below, each experimental diagram requires performing continued measurements during rather long time intervals (normally of the order of 4–6 weeks, depending on the resolution desired). Thus, a direct experimental attempt of locating interesting parameter windows is quite difficult (not to say impossible) task to perform.

We located suitable parameter windows by investigating how the several oscillations generated by the circuit organize themselves in control parameter space. To this

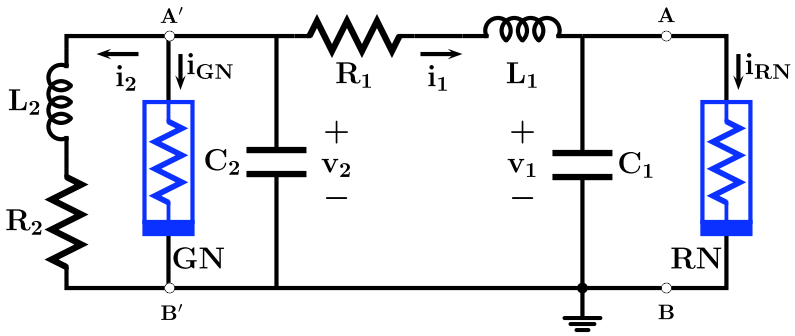

Fig. 1. Schematic representation of the circuit leading to the flow described by Eqs. (1)–(4). The implementation and specific characteristics of the pair of nonlinear resistive components is shown in detail in Fig. 2.

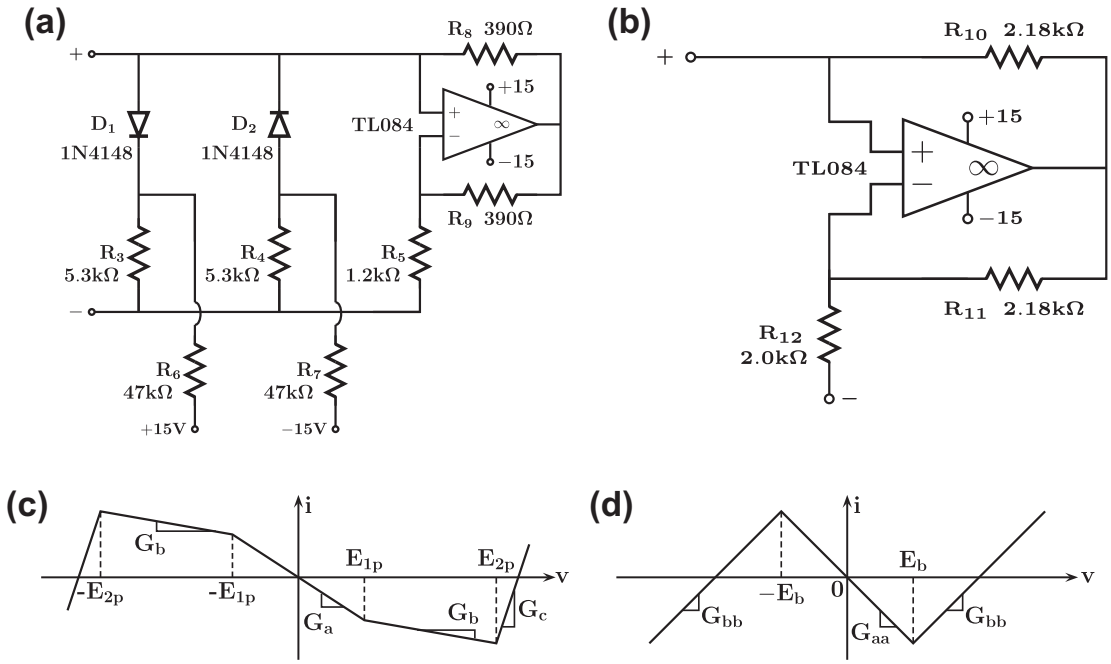

Fig. 2. Schematic representation of the nonlinear elements in the circuit of Fig. 1. Left column: definition of RN and its $v \times i$ characteristic. Right column: definition of GN and its $v \times i$ characteristic.

Table 1
Reference values of the parameters used in our simulations and experiments.

L_1 = 9.8 mH	L_2 = 20.6 mH
C_2 = 12 nF	R_2 = 140 Ω
E_{1p} = 2.5 V	E_{2p} = 11.0 V
E_b = 7.5 V	G_a = −0.7 mS
G_b = −0.5 mS	G_c = 3.35 mS
G_{aa} = −0.5 mS	G_{bb} = 0.5 mS

Table 2
Functional expressions of the experimental quantities and their uncertainties, computed for the values listed in Table 1 and in Fig. 2.

RN circuit	
$E_{1p} = V_\gamma + V_{cc}\frac{R_6}{R_6+R_3}$	$\Delta E_{1p} \simeq 0.3$ V
$E_{2p} = V_{sat}\frac{R_5}{R_5+R_9}$	$\Delta E_{2p} \simeq 4$ V
$G_a = -\frac{1}{R_5}$	$\Delta G_a \simeq 0.1$ mS
$G_b = -\frac{1}{R_5}+\frac{1}{R_6}+\frac{1}{R_3}$	$\Delta G_b \simeq 0.2$ mS
$G_c = \frac{1}{R_8}+\frac{1}{R_6}+\frac{1}{R_3}$	$\Delta G_c \simeq 0.4$ mS
GN circuit	
$G_{aa} = -\frac{1}{R_{12}}$	$\Delta G_{aa} \simeq 0.1$ mS
$G_{bb} = \frac{1}{R_{10}}$	$\Delta G_{bb} \simeq 0.1$ mS
$E_b = V_{sat}\frac{R_{12}}{R_{12}+R_{11}}$	$\Delta E_b \simeq 0.8$ V

end, we solved repeatedly Eqs. (1)–(4) using a standard fourth-order Runge–Kutta algorithm with fixed time step $h = 1 \times 10^{-6}$ s. Following common practice, the first 2×10^5 integration steps were disregarded as due to transient behaviors, with the subsequent 20 $\times 10^5$ steps used to calculate the Lyapunov spectrum (λ_1,λ_2,λ_3,λ_4) corresponding to the four variables of the model.

Each numerically computed panel in Figs. 3 and 4 below displays the analysis of $1200 \times 1200 = 1.44 \times 10^6$ parameter points. This was possible using a cluster of 1536 AMD Opteron on fast processors. Computations were started from the fixed initial conditions $v_1 = 8$ V, $v_2 = -5$ V, $i_1 = -1$ mA, $i_2 = 3$ mA. For each solution we computed the Lyapunov spectrum and counted the number of peaks for selected variables and re-

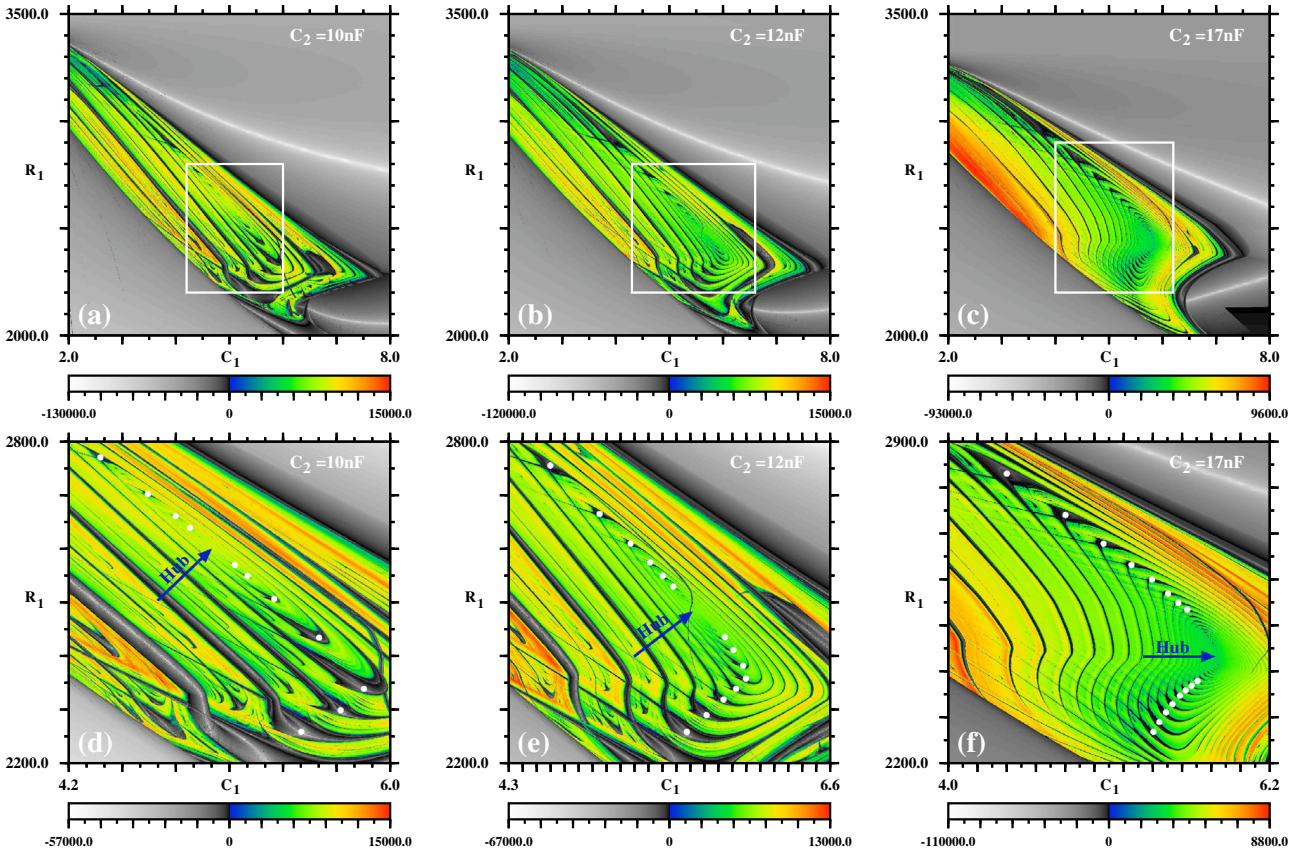

Fig. 3. Lyapunov stability diagrams showing hubs (indicated by arrows) and spirals for (a) C_2 = 10 nF, (b) C_2 = 12 nF, (c) C_2 = 17 nF. Panels (d)-(f) show magnifications of the regions inside the white boxes. White dots are located near shrimp "heads" [16,17], i.e. near points of a double (local) minimum of the exponents. When C_2 increases one sees a clear increase in the density of loops at the bottom of the white boxes, forming a sort of right angle with more and more loops accumulating along the "secondary" diagonal. Units of R_1 and C_1 are Ω and nF.

corded whether pulses repeated or not. To discriminate solutions, we continued integrations for the subsequent 20×10^5 time steps recording up to 800 extrema (maxima and minima) of the variable under consideration, v_2.

4. Stability diagrams

This Section presents stability diagrams for relevant planar sections of the multidimensional parameter surface defined by the circuit. Altogether, such sections anticipate what is to be expected when performing experiments and show how sensitive the results could be as a function of the several parameters involved. We computed two complementary types of stability diagrams, namely stability diagrams characterized either by Lyapunov exponents or by the number of spikes contained in periodic oscillations. These latter diagrams, referred to as "isospike diagrams" [3], are quite helpful to understand how the waveform of the oscillations evolve when parameters are changed but, as shown below, can equally well be used to discriminate chaos from periodicity.

Figs. 3 and 4 present some representative examples of Lyapunov stability diagrams, where the numerical value of the largest non-zero exponents are encoded according to the colorbar[1] shown under the individual panels. In these figures we use colors to represent positive Lyapunov exponents (i.e. chaotic oscillations) while gray shadings encode periodic oscillations, characterized by negative values of the largest non-zero exponent.

Fig. 3 illustrates the unambiguous presence of periodicity hubs and their corresponding spirals in several sections of the parameter control space. It also shows the effect of varying parameters around the reference values listed in Table 1, providing strong evidence of the robustness of the hubs and spirals over quite large ranges of parameters. From Fig. 3 one sees that decreasing C_2 from 12 nF to 10 nF has the effect of increasing the distance between the loops of the spirals, while the opposite effect is observed when increasing C_2 from 12 nF to 17 nF. Note that for these parameters, the two sequences of "shrimps" [16,17] which coil up to form the spiral, with shrimps aligned along two almost perpendicular directions forming a sort of right-angle in the stability diagram. Such arrangement persists when other parameters of the circuit are varied.

Fig. 4 shows Lyapunov stability diagrams and isospike diagrams illustrating the distribution of peaks of the oscillations as observed in the $R_2 \times R_1$ control plane. Since resistors are experimentally easier to control than capacitors or inductors, this parameter plane is particularly attractive to be investigated experimentally. Fig. 4(a) shows a global view of the parameter region containing periodicity hubs and the familiar spiral organization around them.

[1] For interpretation of color in Figs. 4-6, the reader is referred to the web version of this article.

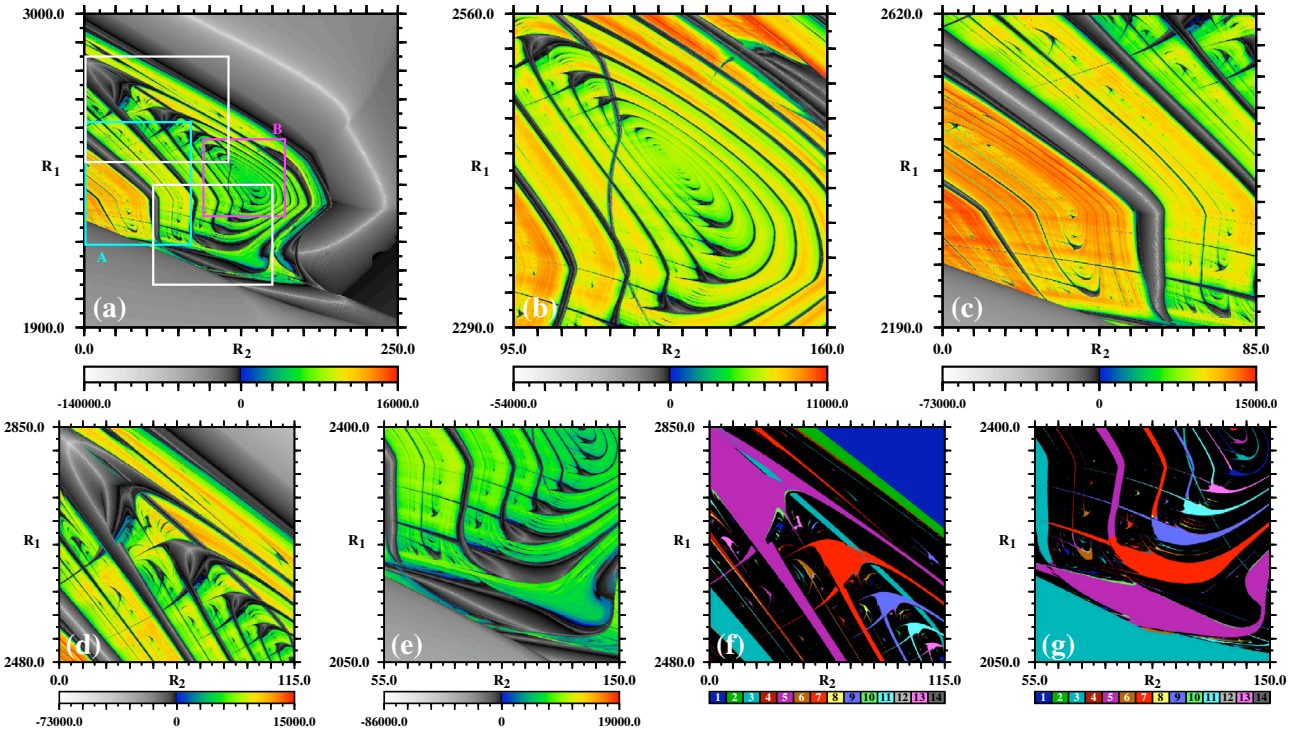

Fig. 4. Hubs and spirals seen on the $R_2 \times R_1$ plane when $L_2 = 20.6$ mH and $C_1 = 6$ nF. (a) Global view of control space. (b) Magnification of box B in (a), showing the main spiral. (c) Magnification of box A in (a), showing Series of secondary spirals. (d) Lyapunov stability diagram illustrating the sequence of shrimps in the upper box in (a). (e) Lyapunov diagram illustrating shrimps inside the lower box in (a). (f) Same as (d), but displaying the number of spikes of the oscillations as observed in $v_2(t)$. (g) Same as (e), but displaying the number of spikes in one period of $v_2(t)$. Units of R_1 and R_2 are Ω. Each individual panel shows the analysis of 1200 × 1200 parameter points.

Fig. 4(b) shows with more details the region near the largest hub while Fig. 4(c) illustrates a region where an apparently infinite quantity of secondary hubs are located. As it is known, an infinite network of hubs and spirals exist in such parameter regions [7].

Fig. 4(d) and (e) show details of the shrimp organization [16,17] far from the hub, converging to it at right angles as seen in Fig. 4(a). From the isospike diagram in Fig. 4(f) one sees that the number of spikes in periodic oscillations of $v_2(t)$ increase by 2 after every turn along the spiral. Fig. 4(g) shows a similar increase along the other sequence of shrimps. Fig. 4(f) and (g) also show the boundaries where changes in the number of peaks occurs when circling along the spiral. An interesting open problem is to investigate what sort of waveform deformations lead to changes in the number of peaks, if changes depend significantly on the specific variable used to count peaks, and if new peaks arise by pulse deformations similar to the ones observed recently in the Mackey–Glass delay-differential equation and in a CO_2 laser [2]. The robust and wide spirals observed in several sections of the parameter space motivated us to investigate the possibility of observing them in a real implementation of the circuit. Such implementation and the results from it are described in the next Section.

Fig. 4(f)–(g) present an independent corroboration of the description above, based on Lyapunov exponents. These figures illustrate the second type of stability diagrams, isospike diagrams, based on the number of spikes contained in one period of the periodic oscillations. Such diagrams can be also used to characterize the periodic or chaotic nature of the oscillations. As indicated by the colorbar, we use 14 colors to represent the number of peaks present in a period of periodic oscillations. Oscillations with more than 14 peaks in one period are plotted "recycling colors mod 14", i.e. taking as their color index the remainder of the integer division of their number of peaks by 14. Multiples of 14 are given the index 14. Lack of numerically detectable periodicity is interpreted as "chaos" and plotted in black. This simple strategy allows all periodic oscillations to be accommodated with a 14 colors palette.

The computation of the isospike diagrams [3] shown in Fig. 4(f)-(g) was done by recording the minima and maxima of the time series together with the instant when they occur. Typically, we used series containing a total of 800 extrema (i.e. 400 maxima and 400 minima). For each parameter value, our computer program records maxima and minima after computing Lyapunov exponents, i.e. after very long transients. We considered that an inflexion point exists whenever the difference between consecutive minima and maxima is larger than a threshold value ϵ. This threshold is used to account for numerical errors and from small fluctuations in the amplitudes, arising from the fact that the numerical integrator may miss "exact" minima and maxima due do the necessity of working with a finite-size step of integration. Although the number of peaks is relatively insensitive to suitably chosen values of ϵ, small differences may arise due to unavoidable errors introduced by the numerical integration. In all isospike diagrams we used $\epsilon = 10^{-6}$.

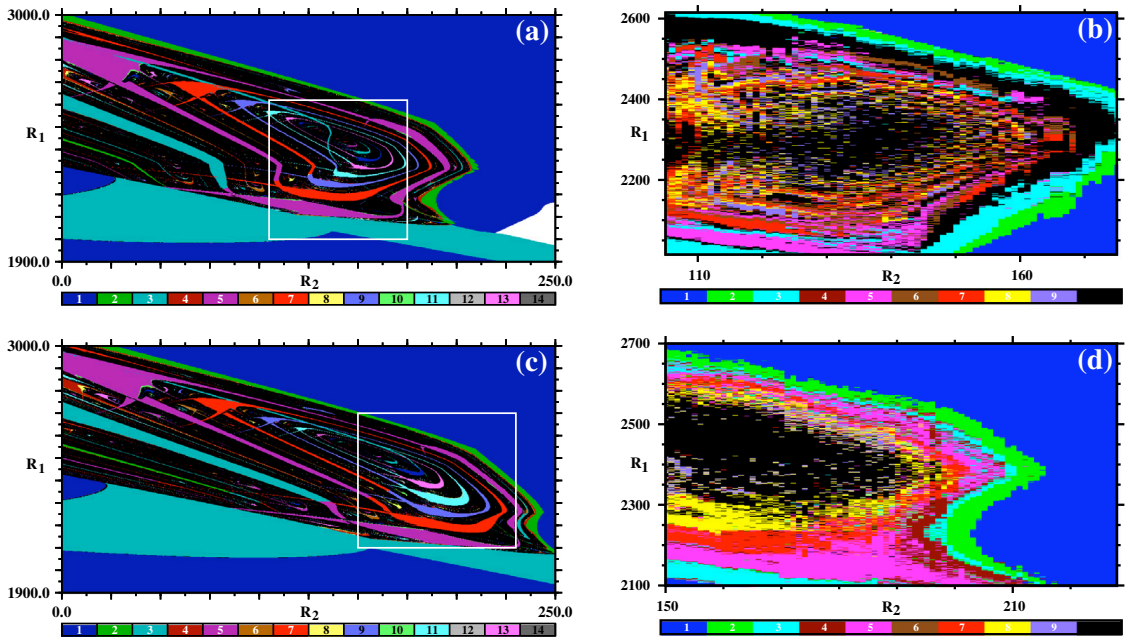

Fig. 5. Comparison between simulations and experiments for two typical inductances: $L_2 = 21.5$ mH (top row) and $L_2 = 23.7$ mH (bottom row). In both cases, $C_1 = 6$ nF. (a) Isospike diagram indicating the distribution of peaks in $v_2(t)$. Black denotes chaos, i.e. lack of periodicity. (b) Experimental distribution of peaks in $v_2(t)$. Resolution: 71 × 601 parameter points. (c) Isospike diagram recording the peaks of $v_2(t)$. (d) Experimental distribution of peaks in $v_2(t)$. Resolution: 79 × 601 parameter points. Units of R_1 and R_2 are Ω. Resolution of numerical simulations: 1200 × 1200 parameter points.

5. Experimental setup and measurements

The oscillator in Fig. 1 was implemented in the laboratory using fast commuting 1N4148 diodes and TL084 operational amplifiers. This operational amplifier was chosen because its chip consists of four amplifiers, in such a way that the circuit could be easily mounted on a board and the nonlinear resistances, *RN* and *GN*, implemented using nearly identical operational amplifiers. The 1N4148 is usually employed in high-frequency applications, with a maximum recovery time of 4 ns. The input voltage of the operational amplifier was maintained constant along the experiment at $V_{cc} = 15.0 \pm 0.6$ V. The other relevant parameter values are $V_\gamma = 0.65 \pm 0.06$ V and $V_{sat} = 12.7 \pm 0.9$ V. Temperature effects on these components are included in the uncertainties mentioned for each component.

In order to build experimental phase diagrams, the resistors R_1 and R_2 were varied electronically over adequate ranges in constant steps of 1 Ω. Due to the parasitic currents inherent in the measurement system, finer resolutions were not possible with the present experimental setup. The parameter space was swept vertically from bottom to top. When starting a new vertical line, all power supplies were disconnected before the value of R_2 was changed. The initial conditions of the variables for each temporal series, which depend on the instantaneous charges of the capacitors, were not controlled, meaning that each new measurement was started from random initial conditions. For each (R_2,R_1) parameter pair, a temporal series of v_2 with 10,000 points, sampled at 250 kHz, was recorded using a Data Acquisition Card (NI-DAQ, USB 6218, 16 bit). For each temporal series, the number of peaks of v_2 is counted and recorded as a marker to discriminate if the pulse was periodic or not. Lack of detectable periodicity was taken as meaning chaos, to which a distinctive marker was assigned.

Fig. 5 presents a comparison between numerical simulations and experimental results (shown in the two rightmost panels) for typical values of the inductance, given in the figure caption. The time required to acquire the data corresponding to a pair (R_2,R_1) was approximately 20 min so that to obtain the values shown in Fig. 5(b) and (d) we needed of the order of 4 to 6 weeks of measurements. During this period, thermal effects due to the heating of the electronic components produced small fluctuations in parameter values. In addition, the inductance and capacitors are slightly sensitive to the different frequencies of operation resulting from changing parameters.

The agreement between the numerical simulations and experimental results seen in Fig. 5 is far from perfect. As mentioned, we believe the lack of agreement to arise as a combined effect of the many uncertainties in the electronic components available to us. It is also possible that the electronic components used might require a slightly different model for them. Errors may also arise during the quite long time interval necessary to collect the data. We could not yet address these issue due to the very long time needed for measurements and to the limited choice of components at our disposal. From Fig. 5 one sees that two major differences between numerical simulations and experimental results exist: First, our grid of resistances could not be tuned finely enough to allow us to unambiguously detect spirals. Thus, only a series of concentric circles is discernible in Fig. 5(b) and (d). Second, all the aforementioned fluctuations end up producing net shifts between the values of the resistors used in simulations and in experiments. Fluctuations are particularly critical near the center of the

spirals as can be recognized in Fig. 5(b) and (d). An important difference between the numerical simulations and our experiments stems from the fact that initial conditions can be precisely fixed in the numerical approach. However, as already mentioned, the initial charges in the capacitors cannot be precisely controlled in the actual experimental procedure. An interesting open question is to find how to reduce the impact of fluctuations and other undesired changes during measurements and to test different models of the components.

6. Conclusions and outlook

We introduced a simple autonomous electronic circuit which contains remarkably wide spirals in its control parameter space. The key property and advantage of this circuit is that its spirals are not compressed and distorted, as it is usual, making them particularly attractive for experimental and theoretical investigations. We computed high-resolution stability diagrams for experimentally accessible parameters and located suitable numerical ranges for the electronic components involved. Recall that, since there is no algorithmic procedure to anticipate the presence of hubs and spirals in models of natural phenomena, the numerical stability diagrams and parameters reported here allow one to bypass lengthy and difficult experimental searches. Concerning the waveforms composing the spirals, they involve infinite families of antiperiodic oscillations, namely oscillations obeying $x(t+T) = -x(t)$, that will be reported elsewhere.

From an experimental point of view, it is important to emphasize that all phase diagrams here refer always to *stability* diagrams, namely to parameter charts reflecting what can be directly measured in the laboratory. Our spirals, represented either with Lyapunov exponents or by counting peaks, should not be confused with another interesting class of mathematical spirals reported recently and connected with *unstable* dynamics. Such spirals are not experimentally observable and require specially devised "painting techniques" [18] for their visualization.

We believe that the use of Lyapunov phase diagrams can significantly augment and speed up the understanding of physical models: diagrams focused just on experimentally measurable features reveal the occurrence of many global bifurcations without recourse to more specialized numerical techniques. They are therefore a very powerful way to begin the analysis of nonlinear systems and can also be applied to laboratory experiments, which, of course, only detect stable structures. A complementary tool that is also useful in analyzing dynamical systems is the direct study of the evolution of the number of peaks and amplitude of the oscillations as parameters are tuned [3] as done in our Fig. 4(f) and (g).

As a final remark, we wish to mention an interesting set of equations with a structure quite similar to our Eqs. (1)–(4) that was recently studied by Tchitnga et al. [19] in this Journal. These authors reported nice experimental evidence of chaos in what they argue to be one of the simplest imaginable autonomous implicit Hartley's oscillator, made with a junction field effect transistor, JFET, and a tapped coil. While the parameter space of the JFET circuit remains to be explored, judging from the structure of its flow it seems likely that the JFET family might also display hubs and spirals. It would be nice to investigate whether this is true or not and how big are such spirals, if any.

Acknowledgements

CC, CB, RG, and ACM acknowledge support from CSIC and PEDECIBA, Uruguay. JGF was supported by FCT, Portugal through the Post-Doctoral Grant SFRH/BPD/43608/2008. JACG was supported by CNPq, Brazil, and by the Deutsche Forschungsgemeinschaft through the Cluster of Excellence *Engineering of Advanced Materials*. The authors thank the Asociación de Universidades Grupo Montevideo for supporting traveling costs. All computations were done in the CESUP-UFRGS clusters in Porto Alegre, Brazil.

References

[1] Bonatto C, Gallas JAC. Phys Rev Lett 2008;101:054101;
Bonatto C, Gallas JAC. Philos Trans R Soc Lond Ser A 2008;366:505.
[2] Junges L, Gallas JAC. Phys Lett A 2012;376:2109;
Junges L, Gallas JAC. Opt Commun 2012;285:4500.
[3] Freire JG, Pöschel T, Gallas JAC. Europhys Lett 2012;100:48002;
Freire JG, Gallas JAC. Phys Chem Chem Phys 2011;13:12191;
Freire JG, Gallas JAC. Phys Lett A 2011;375:1097.
[4] Li XF, Chu YD, Zhang H. Chin Phys B 2012;21:030203.
[5] Vitolo R, Glendinning P, Gallas JAC. Phys Rev E 2011;84:016216.
[6] Freire JG, Gallas JAC. Phys Rev E 2010;82:037202.
[7] For a survey see, Gallas JAC. Int J Bifurcation Chaos 2010;20:197 and references therein.
[8] Sack A, Pöschel T, Lindberg E, Gallas JAC, submitted for publication.
[9] Francke RE, Pöschel T, Gallas JAC. Phys Rev E 2013;87:042907.
[10] Chua LO, Lin GN. IEEE Trans Circuits Syst 1990;37:885.
[11] Chen Wai-Kai. The circuits and filters handbook. Boca Raton: CRC Press; 2003.
[12] Kyprianidis IM, Stoupoulos IN, Haralabidis P, Bountis T. Int J Bifurcation Chaos 2000;8:1903.
[13] Koliopanos CL, Kyprianidis IM, Stoupoulos IN, Anagnostopoulos AN, Magafas L. Chaos Solitons Fract 2003;16:173.
[14] Stoupoulos IN, Miliou AN, Valaristos AP, Kyprianidis IM, Anagnostopoulos AN. Chaos Solitons Fract 2007;33:1256.
[15] Matsumoto T, Chua LO, Komuro M. IEEE Trans Circuits Syst CAS 1985;32:797.
[16] Bonatto C, Garreau JC, Gallas JAC. Phys Rev Lett 2005;95:143905 and references therein.
[17] Lorenz EN. Phys D 2008;237:1689.
[18] Barrio R, Shilnikov A, Shilnikov LP. Int J Bifurcation Chaos 2011;22:1230016.
[19] Tchitnga R, Fotsin HB, Nana B, Fotso PHL, Woafo P. Chaos Solitons Fract 2012;45:306.